Progress In Electromagnetics Research, PIER 88, 39–52, 2008

NEW BENCHMARK RADAR TARGETS FOR SCATTERING ANALYSIS AND ELECTROMAGNETIC SOFTWARE VALIDATION

**D. Escot-Bocanegra, D. Poyatos-Martinez
R. Fernández-Recio, A. Jurado-Lucena
and I. Montiel-Sánchez**

Laboratorio de Detectabilidad
Instituto Nacional de Técnica Aeroespacial
Ctra. Ajalvir Km. 4, 28850, Torrejón de Ardoz, Madrid, Spain

Abstract—A validation process, in which simulations and measurements are compared, is necessary to have confidence in the results obtained by numerical methods that solve scattering problems. This paper presents Radar Cross Section (RCS) measurements of new targets suitable for electromagnetic software comparison and validation. These measurements can be used as an RCS reference data for testing existing and future codes, as well as for the analysis of the scattering mechanisms.

1. INTRODUCTION

In the last 50 years, a very serious effort has been devoted by the scientific community to the development of computational electromagnetic programs, which are gaining place to extensive measurement campaigns aimed to characterize sources of radiation or the scattering of targets [1–6]. These electromagnetic prediction codes have many possibilities to be applied: antenna design, effects of the platforms on their radiation characteristics, Radar Cross Section (RCS) computation or identification and low-observability design among others. In any of these cases, a proper validation process for the determination of the accuracy of the results has to be done. In 1987 an initiative was made in the US, creating the Electromagnetic Code Consortium (EMCC) to consolidate RCS code development. A set of geometries to be used for validating existing codes were measured and published [7, 8]. Apart from this work and other recent effort [9], there are not so many measurements aimed to perform

validation and it is very typical to do it through comparisons against numerical results from other codes and for simple targets which do not show in many cases specific effects that are very interesting to be studied. Moreover, when predictions are used for Non-Cooperative Target Recognition (NCTR), it is very popular to apply the codes to very complex targets obtaining poor results, probably because high order effects are not well reproduced. It is obvious that new targets with medium complexity, but showing specific electromagnetic effects are needed to validate the codes. Comparison with measurements is not only a way to validate codes but also an excellent way to improve the knowledge of the specific EM software with respect to the simulation input parameters, convergence study, etc. In this sense, for instance, input parameters can be adjusted to tune the software tool for the specific necessity of the engineer. In this work new shapes are designed, manufactured, measured and compared with different numerical approaches for validation purposes.

2. RCS MEASUREMENT SYSTEM

2.1. Radar Cross Section

The Far-Field RCS has widely been used to quantify the scattering properties of objects in a radar scenario, and can be described as a measure of power scattered in a given direction when a target is illuminated by an incident wave [10]. It is expressed as

$$\sigma = \lim_{r\to\infty} 4\pi r^2 \frac{|E^{scat}|^2}{|E^{inc}|^2} \tag{1}$$

where E^{scat} is the scattered electric field, E^{inc} is the incident field at the target and r is the distance from the target to the point where the scattered power is measured. The unit for σ is area, in square meters (m^2) or dBsm in logarithmic scale.

2.2. Measurement Method

The configuration used to measure the new targets can be seen in Fig. 1 where the subsystems are presented. Measurements are performed in the frequency domain where the step frequency must be small enough to locate the target inside the maximum unambiguous range. The most suitable reference (flat plate or sphere) is also measured to correct each target depending on its reflectivity level. Several techniques have been applied to diminish the measurement error and maximize the signal-to-noise ratio of the measured signal: software gating, direct

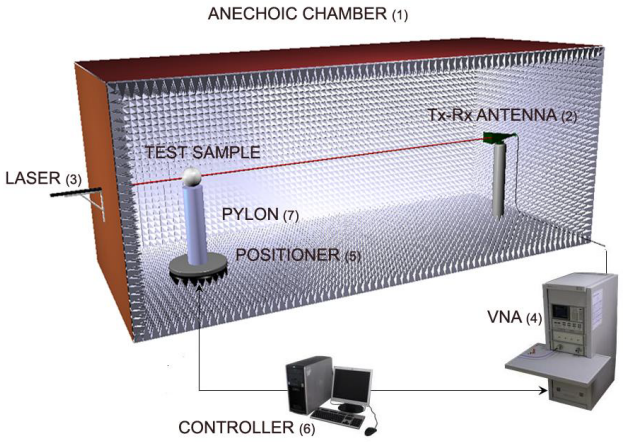

Figure 1. Measurement SetUp. (1): Anechoic Chamber of $3\,\mathrm{m} \times 3\,\mathrm{m} \times 7\,\mathrm{m}$ ($\mathrm{H} \times \mathrm{W} \times \mathrm{L}$). (2): Antenna tx/rx (monostatic configuration). (3): Laser alignment system. (4): Vector Network Analyzer (VNA). (5): Azimuth positioner. (6): PC and control software. (7): Styrofoam pylon and supports.

background subtraction and coherent integration. The measurement distance has been selected to accomplish the far field criterion. Fig. 2 shows the maximum size of the target that can be measured in this facility. Proper environmental conditions for microwave equipment and anechoic chamber maintenance are assured being guaranteed the stability of humidity and temperature. Different types of error (see Table 1) have been estimated following [11], obtaining a maximum overall measurement uncertainty of 0.79 dB.

3. SOFTWARE TOOLS (HFSS, FDTD CODE & FASCRO)

In order to show the utility of these measurements, three electromagnetic prediction codes have been compared with them. The first code is HFSS [12], an h-adaptive commercial code based on the Finite Element Method (FEM). The second one is a code that makes use of the Finite Difference Time Domain (FDTD) [13, 14]. These codes are rigorous methods (or low frequency methods) where a direct discretization of the Maxwell equations in its differential form is performed. The last code is FASCRO, based on the work by [15, 16], which uses a combination of two high frequency techniques: Physical Optics (PO) and Physical Theory of Diffraction (PTD) applied to objects modelled by NURBS surfaces [17–19]. The high frequency

Table 1. Estimated error sources (maximum).

Quantity	Estimation (dB)
VNA Measurement Error	0.4
I-Q Imbalance	incl. in VNA error
Nonlinearity	incl. in VNA error
Frequency	incl. in VNA error
Integration	not applicable
Drift (Temperature Stability, etc.)	negligible
Cross Polarization (Pol. Error)	0.1
Alignment error	0.64
Target Orientation	incl. in alignment error
Average Illumination	incl. in alignment error
Field Non-Uniform. (Near Field)	negligible
Range	negligible
Noise-Background error	negligible
Background-target Interactions	negligible
Reference RCS	0.2
Max. Overall uncertainty (RSS). For $\sigma > -45$ dBsm	**0.79**

Table 2. CPU time and computer memory required by the different codes. All the computations have been carried out on a 3.19 GHz Intel Xeon CPU with 12 GB of RAM.

Target	Code	CPU time (s)	Memory
PRISM	FASCRO	2	12MB
	HFSS error=0.1	342	217MB
	HFSS error=0.01	5193	1.3GB
	HFSS error=0.001	24074	4.7GB
	FDTD	72200	35MB
TRUNCATED CONE	FASCRO	2	12MB
	HFSS error=0.1	446	287MB

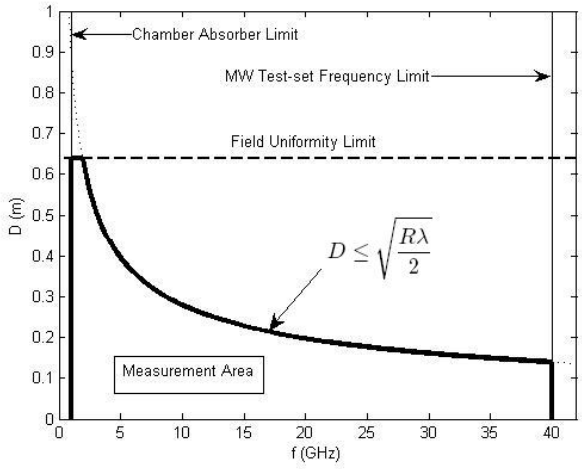

Figure 2. Maximum size of the target (D) vs. frequency for the anechoic chamber of Fig. 1. R is the maximum measuring range of this facility.

methods are obtained from simplifications of the Maxwell equations under the assumption that the scattering object is electrically large. It is worth noting that computing time and memory requirements for the first set of numerical techniques are much higher than for the second one. Table 2 shows CPU times and computer memory required by the different codes for the cases considered in this paper.

4. TARGET DESCRIPTION

The spherical coordinate system used for this work is shown in Fig. 3. The elevation angle (θ) is taken from the positive z-axis and the azimuth angle (ϕ) from the positive x-axis.

4.1. Target Fabrication

The metallic targets are made of aluminium, and were fabricated by a three axis numerically controlled machine (tolerance 0.05 mm). The targets have been made in one piece and neither structural supports nor screws have been used. Adequate foam structures ($\epsilon_r \sim 1$) have also been built to measure the different sweep angles whenever necessary. The targets sizes were designed to fulfil the far field condition in the anechoic chamber up to X-band.

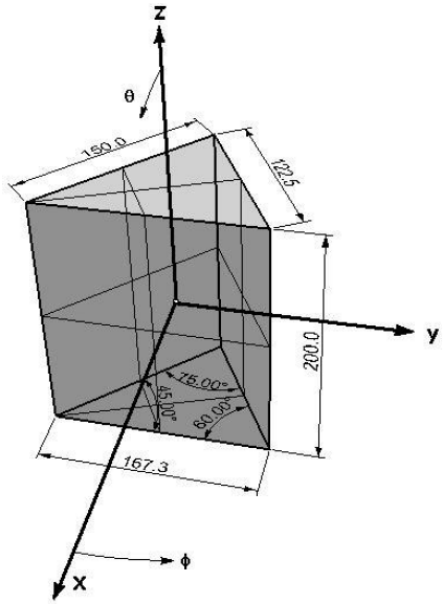

Figure 3. Prism description: size (in mm) and angles (in degrees). The height of the prism is 200mm and the largest face is normal to the x-axis. The sides of the triangular base are 167.3 mm, 122.5 mm and 150 mm.

4.2. Triangular Prism

The first target is a prism with a triangular base oriented along the z-axis and centred in the plane $z = 0$ (see Fig. 3). The objective of this target is to show the RCS response of planar plates of different dimensions. Moreover, diffraction is the dominant effect in the intermediate region between specular responses. Therefore, diffraction from wedges with 45°, 60° and 75° inner angles can be examined. Also note that lengths of the edges for the triangular faces and therefore their diffractions, are different. This target is suitable for validate the modelling of planar facets (either quadrangular or triangular) and straight edges diffraction contribution.

4.3. Truncated Cone

The other target is an end-capped truncated cone oriented along the z-axis and centred in the plane $z = 0$ (see Fig. 4). There are several interesting points in this target. First, it shows the RCS response of targets with single curvature (common in structural parts

of aircrafts, such as the fuselage). It is also important to know the diffraction mechanism in curved edges. Reflection from planar surfaces with curved edges can also be observed. Therefore, this target is especially suitable for the validation of the prediction of objects with flat surfaces delimited by curved edges and for evaluation of curved edges contribution. These scattering mechanisms can be observed in a cylinder but the truncated cone constitutes a further step in complexity.

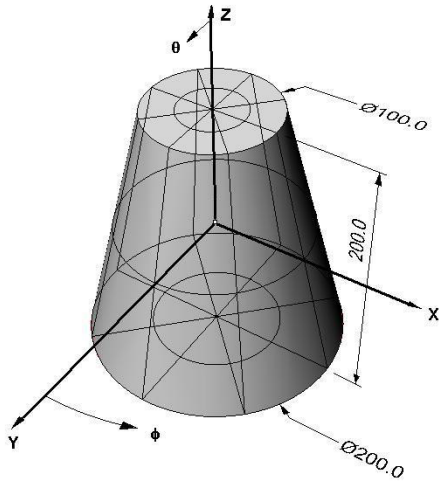

Figure 4. Truncated cone description: size (in mm). The height of the target is 200 mm. The major diameter is 200 mm and the minor one is 100 mm.

5. MEASUREMENTS AND SIMULATIONS

5.1. Triangular Prism Results

The prism has been measured from 5 to 13 GHz. RCS cuts have been measured for vertical (VV) and horizontal (HH) polarizations. The first RCS pattern, labelled as C1, corresponds to $\theta = 90°$ and ϕ ranging from 0° to 360° with a 1° step. The second one, labelled as C2, refers to $\phi = 90°$ and θ ranging from 0° to 360° with a 1° step.

The first RCS pattern C1 for VV polarization at 8 GHz is plotted in Fig. 5. Three specular lobes are clearly defined and correspond to the three quadrangular faces. Each face has a different area, so the corresponding RCS level is also different. Results from FASCRO are also shown and a very good agreement is found. Both effects,

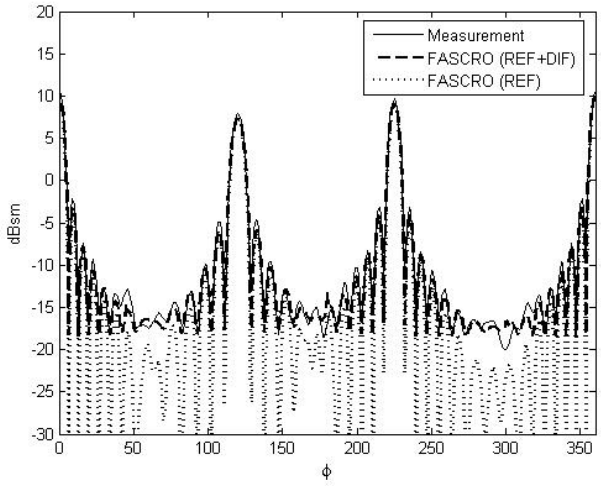

Figure 5. RCS pattern of the prism (C1). Frequency 8 GHz. Polarization VV. Comparison with FASCRO.

reflection and diffraction, are needed to obtain a good result with FASCRO and from here now all FASCRO simulation results include both reflection and diffraction mechanisms. As it has been mentioned above, measurements are very useful to tune the different parameters of the electromagnetic software. For instance, a variation of the stopping error criterion of the simulation can be performed for HFSS (FEM code) as it is shown in Fig. 6. The smaller the convergence error, the better the accordance between HFSS and measurements. An error of 0.1 can be enough for most applications. Only small differences in the region where the diffraction is the main scattering mechanism can be appreciated.

Comparison with a FDTD code is depicted in Fig. 7 at 10 GHz. Good agreement is found except for particular directions such as 90°, 180° and 270°. This discrepancy is due to the fact that the unit cell of the mesh generated by the FDTD code is cubic in shape and so they do not conform to scatterers with wedges as in this case. Therefore, spurious responses appear in these directions (the sides of the small cubes are oriented along them). This result is useful to evaluate the code and to bear in mind this disadvantage for future predictions. Nevertheless, in the other directions, agreement is good.

The RCS patterns for the other cut, C2, for VV and HH polarizations at 7 GHz can be seen in Fig. 8 and 9. FASCRO prediction is also plotted and good agreement is found. Depending on the application, the errors in the low levels can be negligible.

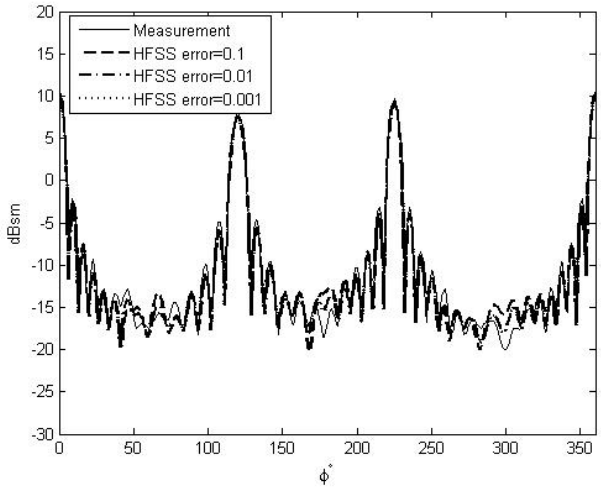

Figure 6. RCS pattern of the prism (C1). Frequency 8 GHz. Polarization VV. Comparison with HFSS.

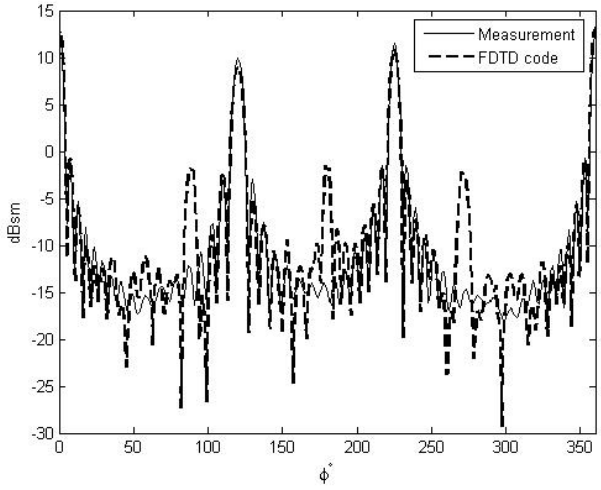

Figure 7. RCS pattern of the prism (C1). Frequency 10 GHz. Polarization VV. Comparison with a FDTD code.

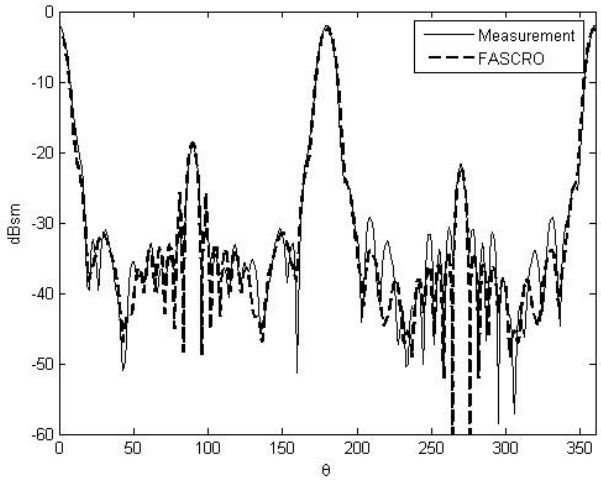

Figure 8. RCS pattern of the prism (C2). Frequency 7 GHz. Polarization VV. The specular lobes are not symmetrical due to the different lengths of the triangular faces.

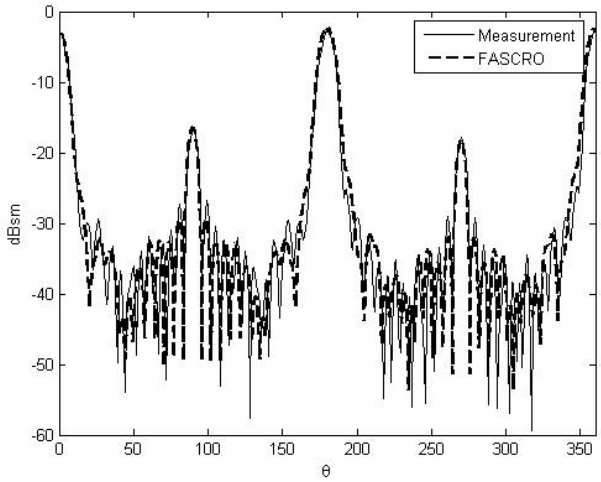

Figure 9. RCS pattern of the prism (C2). Frequency 7 GHz. Polarization HH.

5.2. Truncated Cone Results

The truncated cone has been measured from 5 to 13 GHz. The RCS pattern, for VV and HH polarizations, corresponds to $\phi = 0°$ and θ ranging from 0° to 180° with a 1° step.

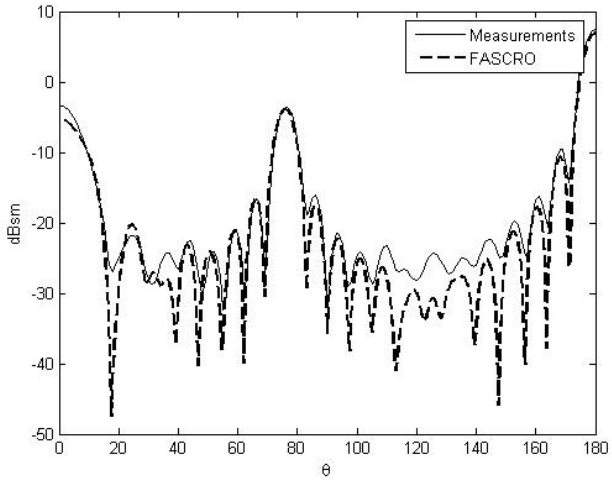

Figure 10. RCS pattern of the truncated cone. Frequency 6 GHz. Polarization VV.

Figure 10 shows the RCS pattern for VV polarization at 6 GHz. Three main lobes are clearly defined. Two of them correspond to the specular reflection from the two bases. The minor one corresponds to $\theta = 0°$ and the major one to $\theta = 180°$ (see Fig. 4). Different levels can be appreciated due to the different areas of the corresponding bases. The other main lobe corresponds to the angle at which the generatrix is perpendicular to the incident direction. Diffraction from the curved edges becomes important in the intermediate region between the main lobes. Results from FASCRO are also shown and good agreement is found, especially in the main and lateral lobes. Small discrepancies are found between $\theta = 100°$ and $150°$. This is due to the fact that FASCRO does not incorporate the diffraction mechanisms from curved edges. These contributions are especially relevant in the areas of low RCS level. Therefore, it corresponds to the engineer to decide if this precision is enough for her or his application. For sake of completeness, measurements for the HH polarization are given in Fig. 11 and comparison with HFSS (FEM code) shows very good agreement. FEM, as a rigorous method, takes into account the diffraction mechanisms.

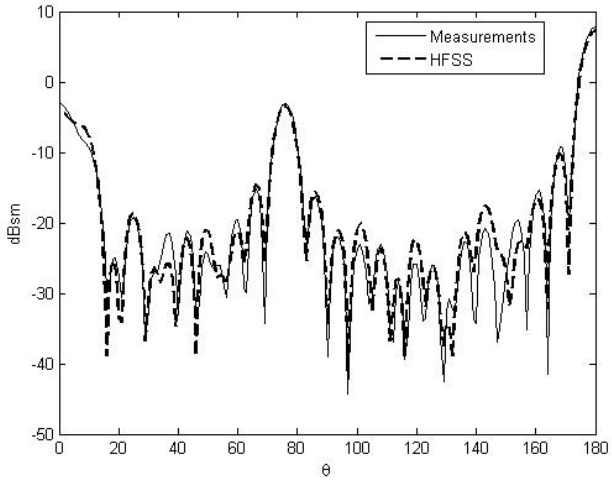

Figure 11. RCS pattern of the truncated cone. Frequency 6 GHz. Polarization HH.

6. CONCLUSIONS

Measurements presented in this paper constitute a contribution for the RCS community and can be used as a valuable tool to validate and to adjust the input parameters of EM prediction codes according to the requirements of the engineer. Discrepancies found between measurements and predictions have been discussed and appropriate explanations have been given.

ACKNOWLEDGMENT

The authors would like to thank Juan Ángel Aguilar Rosado and General Workshops of INTA for their help in the design and fabrication of the targets. This work has been supported by INTA under the Electronic Warfare and Non Cooperative Target Identification project.

REFERENCES

1. Vinogradov, S. S., P. D. Smith, J. S. Kot, and N. Nikolic, "Radar cross-section studies of spherical lens reflectors," *Progress In Electromagnetics Research*, PIER 72, 325–337, 2007.
2. El-Ocla, H., "On laser radar cross section of targets with large

sizes for E-polarization," *Progress In Electromagnetics Research*, PIER 56, 323–333, 2006.

3. Jin, K. S., T. I. Suh, S. H. Suk, B. C. Kim, and H. T. Kim, "Fast ray tracing using a space-division algorithm for RCS prediction," *Journal of Electromagnetic Waves and Applications*, Vol. 20, No. 1, 119–126, 2006.
4. Yuan, N., T. S. Yeo, X. C. Nie, and L. W. Li, "RCS computation of composite conducting-dielectric objects with junctions using the hybrid volume-surface integral equation," *Journal of Electromagnetic Waves and Applications*, Vol. 19, No. 1, 19–36, 2005.
5. Wei, X. C., E. P. Li, and Y. J. Zhang, "Application of the improved finite element-fast multipole method on large scattering problems," *Progress In Electromagnetics Research*, PIER 47, 49–60, 2004.
6. Jung, B. H., T. K. Sarkar, and Y. S. Chung, "A survey of various frequency domain integral equations for the analysis of scattering from three-dimensional dielectric objects," *Progress In Electromagnetics Research*, PIER 36, 193–246, 2002.
7. Woo, A. C., H. T. G. Wang, M. J. Schuh, and M. L. Sanders, "Benchmark plate radar targets for the validation of computational electromagnetics programs," *IEEE Antennas and Propagation Magazine*, Vol. 34, No. 6, 52–56, 1992.
8. Woo, A. C., H. T. G. Wang, M. J. Schuh, and M. L. Sanders, "Radar targets for the validation of computational electromagnetics programs," *IEEE. Antennas and Propagation Magazine*, Vol. 35, No. 1, 84–89, 1993.
9. Workshop EM radar signatures 2008. Toulouse, France. http://www.isae.fr/fr/acces_directs/workshop_radar_signatures_2008.html
10. Knott, E. F., J. F. Schaeffer, and M. T. Tuley, *Radar Cross Section*, Artech House, 1993.
11. IEEE Std 1502TM-2007, "IEEE recommended practice for radar cross-section test procedures," IEEE Antennas and Propagation Society, Sept. 2007.
12. HFSS^{TM} v11. ANSOFT. Jul. 2007, http://www.ansoft.com
13. Taflove, A. and K. R. Umashankar, "The finite-difference time-domain (FD-TD) method for numerical modeling of electromagnetic scattering," *IEEE. Trans. on Magnetics*, Vol. 25, No. 4, 3086–3091, 1989.
14. Gong, Z. Q. and G. Q. Zhu, "FDTD Analysis of an anisotropically

coated missile," *Progress In Electromagnetics Research*, PIER 64, 69–80, 2006.

15. Perez, J. and M. F. Catedra, "Application of physical optics to the RCS computation of bodies modelled with NURBS surfaces," *IEEE. Trans. on Antennas and Propagation*, Vol. 42, No. 10, 1404–1411, 1994.
16. Conde, O. M., J. Perez, and M. F. Catedra, "Stationary phase method application for the analysis of radiation of complex 3-D conducting structures," *IEEE. Trans. on Antennas and Propagation*, Vol. 49, No. 5, 724–731, 2001.
17. Zhao, Y., X. W. Shi, and L. Xu, "Modeling with NURBS surfaces used for the calculation of RCS," *Progress In Electromagnetics Research*, PIER 78, 49–59, 2008.
18. Chen, M., X. W. Zhao, Y. Zhang, and C. H. Liang, "Analysis of antenna around NURBS surface with iterative MOM-PO technique," *Journal of Electromagnetic Waves and Applications*, Vol. 20, No. 12, 1667–1680, 2006.
19. Chen, M., Y. Zhang, and C. H. Liang, "Calculation of the field distribution near electrically large NURBS surfaces with physical-optics method," *Journal of Electromagnetic Waves and Applications*, Vol. 19, No. 11, 1511–1524, 2005.